Available online at www.sciencedirect.com

ScienceDirect

ELSEVIER

International Journal of Mass Spectrometry 269 (2008) 112–117

International Journal of Mass Spectrometry

www.elsevier.com/locate/ijms

Secondary ion mass spectrometry with C_{60}^+ and Au_{400}^{4+} projectiles: Depth and nature of secondary ion emission from multilayer assemblies

Zhen Li, Stanislav V. Verkhoturov, Jay E. Locklear, Emile A. Schweikert *

Department of Chemistry, Texas A&M University, College Station, TX 77843-3144, USA

Received 21 August 2007; received in revised form 26 September 2007; accepted 26 September 2007
Available online 5 October 2007

Abstract

Alternating nanometric thin layer films made from poly(diallyldimethylammonium chloride), poly(styrene sulfonate) and montmorillonite clay were analyzed with 26 keV C_{60}^+ (433 eV/atom) and 136 keV Au_{400}^{4+} (340 eV/atom). Secondary ion (SI) emission depth from such thin films was determined to be ∼6–9 nm with C_{60}^+ bombardment. Similar depth of emission was also reported with Au_{400}^{4+} projectile impacts [Z. Li, S.V. Verkhoturov, E.A. Schweikert, Anal. Chem. 78 (2006) 7410]. The SI spectra contain recoiled C_{60} projectile constituents (*m*/*z* = 12, 13, 36). They track the compositional variation of the assembled thin layers except for C^- and CH^- whose abundances appear to correlate with the presence of metal atoms in the topmost layer.
© 2007 Elsevier B.V. All rights reserved.

Keywords: Secondary ion mass spectrometry; Cluster projectile; Emission depth; Layer-by-layer film; Recoil

1. Introduction

Large cluster projectiles (e.g., C_{60}^+, Au_{400}^{4+}) have become well recognized as advantageous projectiles for secondary ion mass spectrometry (SIMS) [1–8]. The scope of large cluster bombardment can be assessed in terms of: (a) secondary ion (SI) yields which are enhanced in comparison to equal velocity mono or small polyatomic projectiles; (b) the depth of emission of SIs; and (c) the accuracy of the SI signal. This study presents a contribution on the latter two issues with results obtained under 26 keV C_{60}^+ and 136 keV Au_{400}^{4+} bombardments. The projectiles had comparable impact energies at 433 and 340 eV/atom, respectively. The depth of SI emission was examined on samples consisting of alternating nanometric layers of oppositely charged polyions, poly(diallyldimethylammonium chloride)-PDDA, poly(styrene sulfonate)-PSS and montmorillonite clay. Several papers describe the properties and characteristics of such multilayer thin films [9,10]. Given their chemical compositions and densities, these assemblies simulate polymeric and biological materials. The layered assemblies allowed also to assess the accuracy with which the SI signals track the compositional variation. We report here on signals affected by recoiled atoms from C_{60} projectile and on an unexpected reversal in the intensities of the C^- and CH^- emissions from successive nanolayers. These observations are compared below with data obtained on duplicate samples from Au_{400}^{4+} impacts. The SIs examined are of low *m*/*z*, i.e., signals that are abundant in the emission from organic, polymeric and biological materials. The experiments described below were performed in the event-by-event bombardment/detection mode, where a sequence of individual projectiles each strike an unperturbed area of the target, i.e., a manner analogous to how molecular dynamic (MD) simulations are carried out [11,12].

2. Experimental

2.1. Mass spectrometer

A custom-built C_{60}^+ ion source coupled with time-of-flight mass spectrometer (Fig. 1) was used for the analysis of the layer-by-layer thin films. The C_{60} instrument has been described previously [13,14]. The C_{60}^+ ions were accelerated to +16 keV towards a negatively biased target (−10 keV), which resulted in a total impact energy of 26 keV. The setup used for the experiments with Au_{400}^{4+} projectiles has been described elsewhere [7,8]. A key feature of both instruments is the event-by-event

* Corresponding author. Tel.: +1 979 845 2341; fax: +1 979 845 8156.
E-mail address: Schweikert@mail.chem.tamu.edu (E.A. Schweikert).

1387-3806/$ – see front matter © 2007 Elsevier B.V. All rights reserved.
doi:10.1016/j.ijms.2007.09.018

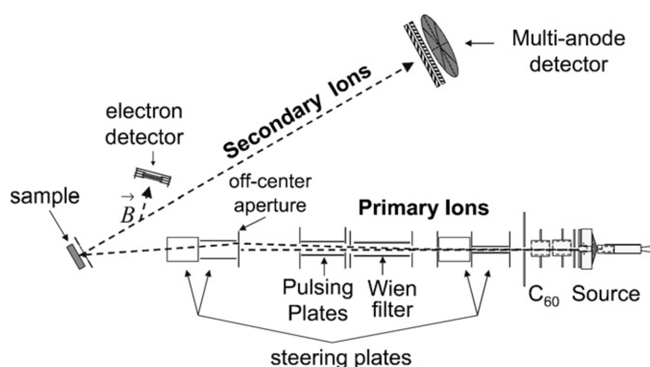

Fig. 1. Schematic of the C_{60} effusion source time-of-flight mass spectrometer.

mode bombardment/detection. Under such condition, individual primary projectiles impact the sample surface in a discrete manner. There is no overlap in time or space between successive projectiles. Secondary ions resulting from single projectile impacts are stored individually as singular events. Each spectrum is a summation of at least 1×10^6 such events over an impact area of ~1 mm^2. Secondary ions ejected are detected by a dual micro-channel plate (MCP) assembly with an 8-anode detector to improve detection efficiency [7,13]. The SI data are collected and analyzed with Total Matrix of Events (TME) software developed for event-by-event detection [15]. For a given secondary ion A, the percentage yield Y_A is calculated as follows:

$$Y_A\,(\%) = 100\sum_{x_A}\frac{x_A I(x_A)}{N} = 100\sum_{x_A} x_A P(x_A)$$

where x_A is the number of SIs of type A detected simultaneously per single impact/emission event ($0 \le x_A \le 8$); $I(x_A)$ is the number of events where ions A are detected; and N is the total number of projectile impacts. $P(x_A)$ is the probability distribution of the number of ions A detected per impact/emission event.

2.2. Materials

Poly(diallyldimethylammonium chloride)-PDDA, MW = 100,000–200,000, 20% water solution and poly(styrene sulfonate)-PSS, MW = 70,000 were obtained from Sigma–Aldrich (Milwaukee, WI). Polymer stock solutions with concentrations of 5 mg/mL and 0.5 M NaCl were used for film assembling. Montmorillonite clay (STx-1, $(Ca_{0.27}Na_{0.04}K_{0.01})[Al_{2.41}Fe(III)_{0.09}Mg_{0.71}Ti_{0.03}][Si_{8.00}]O_{20}(OH)_4$) was purchased from The Source Clays Repository (Purdue University, West Lafayette, IN) and purified according to literature [10]. The clay solution used for film assembling was 0.5 mg/mL. Water was purified by Milli-Q system (Millipore, Billerica, MA) with a specific resistance of 18.2 MΩ cm.

2.3. Film assembling

The films were assembled via the layer-by-layer film assembling technique [9] on 1 cm × 1 cm silicon wafer substrates (Waferworld, West Palm Beach, FL). The Si pieces were cleaned with *Piranha Solution* (3:1, v:v, 98% H_2SO_4:30% H_2O_2) at 70 °C for 15 min and washed with copious amounts of water. The cleaned wafer was dipped into PDDA stock solution for 10 min, the resulting film was a 1-layer film. To obtain a 2-layer film, a 1-layer film was dipped into PSS stock solution for 10 min. For films with more than 3 layers, a wafer with an initial 2-layer film was dipped alternately into PDDA and clay stock solutions. Thus, PSS, which was used as the indicator layer, was always located at the 2nd layer of the assembly with a varying number of PDDA and clay layers on top. A rinsing and drying step was carried out after each dipping step to remove loosely bound material. One up to 12-layer films were assembled and tested. The thickness of each assembled layer ranges from less than 1 to 4 nm. A thickness calibration curve obtained from previous experiments was used to estimate the thickness of the thin layer films [8].

2.4. XPS

X-ray photoelectron spectrometry (XPS) experiments were performed in the Materials Characterization Facility at Texas A&M University with a Kratos Axis Ultra Imaging XPS (Kratos Analytical, Chestnut Ridge, NY). The same set of 1–12-layer films used for SIMS analysis were tested with XPS for elemental composition information.

3. Results and discussion

3.1. Depth of SI emission

As mentioned above, PSS served as the indicator layer to test the depth of SI emission. Mass spectra from 2 and 4-layer assemblies are shown in Fig. 2. The peak of interest for locating PSS is that of its monomer at m/z = 183. Its signal decreases radically from the 2 to the 4-layer assembly. The yield data plotted in Fig. 3 show that the PSS signal disappears for 6-layer film and beyond.

The distance between the top of the PSS indicator layer and the 5th PDDA layer is ~6 nm, while the distance between the PSS and the 6th clay layer is ~9 nm. Thus for the assemblies studied here, the SI emission depth is between 6 and 9 nm under 26 keV C_{60}^+ projectile impacts. A similar depth of emission has been reported when Au_{400}^{4+} projectiles of roughly comparable velocity impact these thin layer films [8]. A MD simulation of 5 keV C_{60} impacts on an organic surface shows a penetration depth of ~5 nm [11]. These computer simulations also indicate the crater formed after impact has a semispherical shape with ~15 nm in diameter and target constituents are emitted from a depth of ~10 nm.

The depth of emission can also be assessed by plotting the yield of SIs due to clay: SiO_2OH^- at m/z = 77 and $Al_2O_3SiO_2OH^-$ at m/z = 179. Fig. 4 shows that the signal at m/z = 179 is solely from the clay layer, indeed no signal above background is observed for 1–3-layer films when clay is absent. The yields of m/z = 179 increase by ~30% between the 4 and 6-layer films, which indicates a contribution from the clay in the 4th layer to the SI signal. The signals tend to level off for 8, 10 and 12-layer films, suggesting that ions at m/z = 179 are

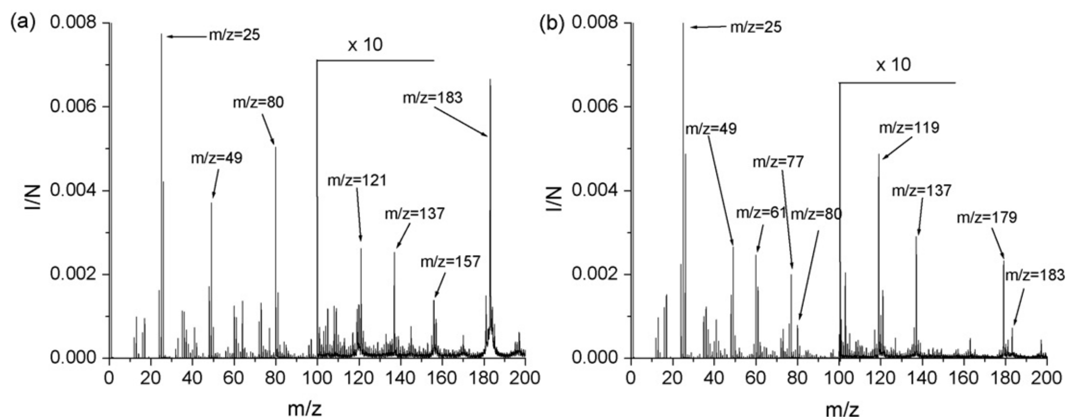

Fig. 2. Negative ion mass spectra of: (a) 2-layer PDDA/PSS film and (b) 4-layer PDDA/PSS/PDDA/clay film analyzed with 26 keV C_{60}^+ projectile. Counts are normalized to the total number of events (~1×10^6).

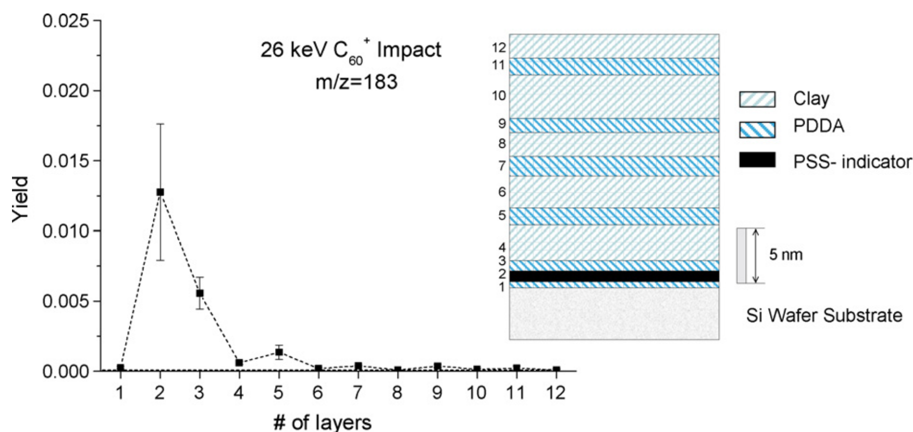

Fig. 3. SI yields of ions $m/z = 183$ vs. the number of layers. An illustration of the structure of a 12-layer film is shown on the right.

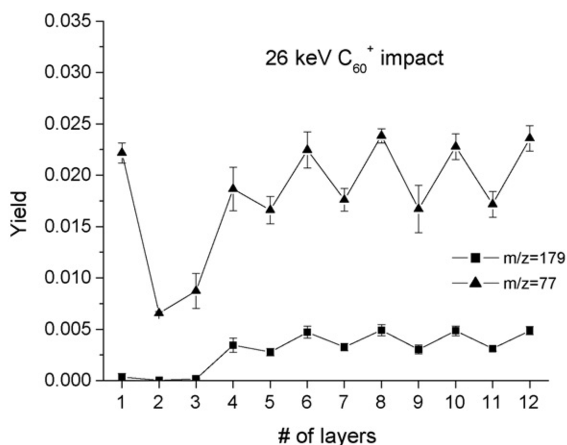

Fig. 4. Oscillation of negative SI yields $m/z = 77$ (SiO_2OH^-) and 179 ($Al_2O_3SiO_2OH^-$) with the number of layers.

due mostly to the two topmost clay layers. The oscillation in the $m/z = 179$ yield illustrates the sensitivity of SIMS to surface composition. It should be noted that $m/z = 77$ originates from the Si wafer for the low thickness films, but reflects only the presence of clay in the larger scale assemblies in a similar fashion to that observed for $m/z = 179$.

3.2. Evaluation of film quality

Most SIs observed in the mass spectra show oscillation in a level range similar to that of $m/z = 179$. An exception to this trend is observed for ions $m/z = 35$, which are assigned to $^{35}Cl^-$. The chlorine ions are counter ions for the positively charged PDDA layers. The yield is higher for the odd numbered layers, i.e., when PDDA is the topmost layer. In contrast to the plateau observed for the yield of ions $m/z = 77$ and 179 (Fig. 4), the yield for ions $m/z = 35$ keeps increasing for successive odd numbered layers (Fig. 5 left axis). This trend is confirmed with XPS which shows an increase in the surface concentration of chlorine in successive PDDA layers (Fig. 5 right axis). The information depth of XPS for an organic surface is in the range of 4–10 nm [16] and thus comparable to the depth of SI emission.

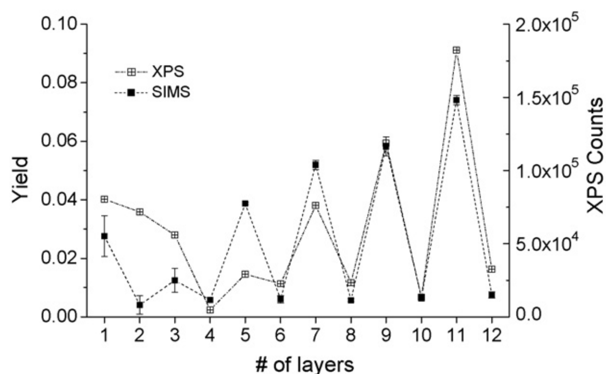

Fig. 5. SI yields of $^{35}Cl^-$ (left axis) and XPS counts of Cl (right axis) vs. the number of layers. SIMS results were obtained with 26 keV C_{60}^+ bombardment.

It has been shown that layer-by-layer films have "self-healing" properties, i.e., defects occurring at the initial stage of assembling disappear with successive addition of overlayers [17]. The overall smoothness of the films increases with the number of layers assembled with a concomitant reduction in the total surface area. A steady state of SI yields is observed after the 8th layer for ions from clay ($m/z = 77$ and 179). This indicates the packing densities of film components remain constant with successive layer addition. Thus, a higher surface charge density is required to maintain a stable assembly with reduced surface area. The observation of increased Cl surface concentration from XPS and SIMS experiments suggests an increased surface charge density, and thus a better quality of the films as more layers are assembled. Again, SI signals at $m/z = 35$ oscillate with the alternation of the topmost layers. This suggests most of the chlorine signals observed in SIMS originate from the topmost thin layer of the sample surface.

3.3. *Influence of recoiled projectile constituents on yield oscillations*

The data presented so far and those published previously [8], show an oscillation of the SI yield reflecting the characteristics of the topmost layer (chemical composition, thickness).

A more complicated behavior of oscillations is observed for small carbon and hydrocarbon ions (Fig. 6). First, the amplitude of oscillations decreases remarkably in the case of C_{60}^+ bombardment. Second, a reversed even/odd oscillation is observed for C^- and CH^- ions in the case of Au_{400}^{4+} projectile impacts (Fig. 6a and b). The yields of these ions are higher when the clay layer is the topmost layer despite the absence of hydrocarbons in clay. The "expected" order of oscillations is observed for C_2H^- and larger cluster ions (Fig. 6c).

We can quantify the SI yield oscillations with the average ratio, K, of high yields, $Y_i^{(\text{high})}$, to adjacent low yields, $Y_i^{(\text{low})}$:

$$K = \frac{1}{n}\sum_{i}^{n} Y_i^{(\text{high})} / Y_i^{(\text{low})}$$

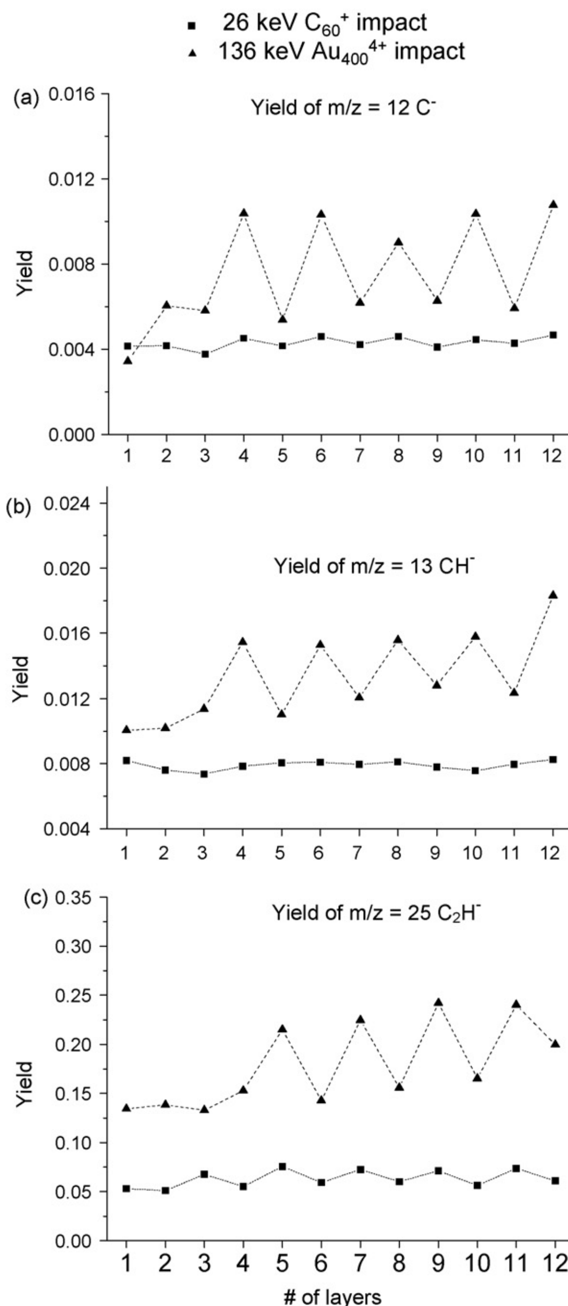

Fig. 6. SI yields of $m/z = 12$, 13 and 25 vs. the number of layers obtained from bombardment with 26 keV C_{60}^+ and 136 keV Au_{400}^{4+} projectiles. The C_{60} and Au_{400} TOF-SIMS instruments have similar transmission and detection efficiencies.

The K values are calculated for 5-layer films and beyond, where the films have long term stability; n refers to the number of peak-to-valley pairs. The value of n equals 4, as there are 4 layer pairs between the 5-layer and the 12-layer films. Table 1 shows the K values for different SIs generated by 26 keV C_{60}^+ (433 eV/atom) and 136 keV Au_{400}^{4+} (340 eV/atom) projectile impacts.

The K values are ~1 for small carbon clusters such as C^-, C_2^-, C_3^- and CH^- in the case of C_{60}^+ bombardment. The absence of "layer-specific" oscillation suggests that the carbon and small carbon cluster ions are mostly due to recoiled

Table 1
Average ratio of yields (K) for selected SIs with 26 keV C_{60}^+ and 136 keV Au_{400}^{4+} projectile impacts

		26 keV C_{60}^+	136 keV Au_{400}^{4+}
$m/z = 12$	C^-	1.09	1.71
$m/z = 13$	CH^-	1.01	1.35
$m/z = 24$	C_2^-	1.09	1.09
$m/z = 25$	C_2H^-	1.24	1.40
$m/z = 26$	CN^-	2.68	1.97
$m/z = 35$	$^{35}Cl^-$	8.56	14.7
$m/z = 36$	C_3^-	1.10	1.48
$m/z = 37$	$^{37}Cl^-$ or C_3H^-	3.27	6.94
$m/z = 77$	SiO_2OH^-	1.36	1.74
$m/z = 179$	$Al_2O_3SiO_2OH^-$	1.59	1.91

The accuracy of measuring SI yield oscillation is ±2%.

projectile constituents [18]. Evidence of projectile constituents recoiling as ions with low kinetic energy has been observed previously in the mass spectrum of secondary ions from an organic surface bombarded with SiF_5^- [19]. A possible mechanism was discussed by Shapiro and Tombrello [20]. One should note that the present experiment and the SiF_5^- experiment were both performed in the "super-static" regime with extremely low doses of bombardment (~10^6 projectiles/mm^2) where the projectile strikes an unperturbed area of the target. Thus, the presence of recoiled CH^- ions (no oscillations) (Fig. 6b, Table 1) indicates the extensive recombination processes in the expanding nanovolume of upward moving atoms, fragments of the analyte and the shattered projectile. These results are consistent with recent MD simulations of C_{60} bombardment of hydrocarbon targets [11,12]. Concurrently, strong oscillations ($K > 1$) observed for small carbon and hydrocarbon clusters in the case of Au_{400}^{4+} bombardment show that these clusters are secondary ions emitted from topmost layers.

Another indication of recoil emission and recombination is obtained from the comparison of yields of Cl^- ($m/z = 35$ and 37) and C_3H^- ($m/z = 37$). As mentioned above, the chlorine is present in the PDDA layers (odd topmost layers) as counter ion. However, the ratio of yields $Y(m/z = 35)/Y(m/z = 37)$ is lower than the isotopic ratio of $^{35}Cl/^{37}Cl = 3.12$ for both projectiles (Fig. 7). But, the ratios are always lower for C_{60} bombardment due to the contribution of C_3H^- recoils (Fig. 7).

The most intriguing observation related to the yield oscillations is the reversed even/odd oscillations for C^- and CH^- ions with Au_{400}^{4+} projectile impacts (Fig. 6a and b). This observation suggests a complex interaction process in the expansion volume resulting in a variety of emission/ionization mechanisms for different emitted species. Considering the depth of emission (~6–9 nm), it appears that the topmost clay layer does not screen the polymer layer below, hence the presence of polymer fragments in the collective outward motion and ion emission. Perhaps, the C and CH neutrals with low electron affinity (1.26 and 1.24 eV, respectively) are ionized effectively by electron exchange processes, when colliding in the plume with metal atoms. In this scenario, the topmost clay layer provides the metal atoms that enhance the ionization probability of C and CH. The mechanism proposed here is similar to that involved in the secondary ion yield enhancement stimulated by metal deposition on the surface of analyte [21]. The effectiveness of the interaction is reduced when the polymer layer is on the top and the clay layer is on the bottom of the interaction volume. In this case the fast moving carbon atoms and small fragments exit the expansion volume without interactions with metal atoms from the layer below. Larger carbon clusters and hydrocarbons have high electron affinities (>3 eV) resulting in higher ion yields regardless of the nature of the topmost layer.

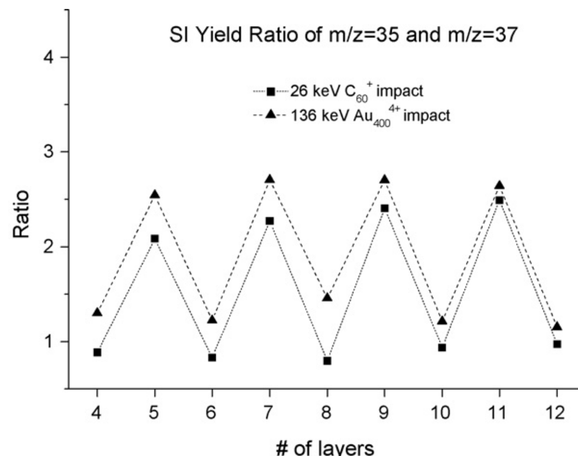

Fig. 7. SI yield ratio of ions $m/z = 35$ and 37 with 26 keV C_{60}^+ and 136 keV Au_{400}^{4+} impacts.

4. Conclusions

The SI yields measured in this study range from 0.001 to 0.2 (0.1–20%). The yields obtained with Au_{400}^{4+} are roughly twice or more as those measured with C_{60}^+, with the two projectiles of comparable impact velocities. The SI yields illustrate the high detection sensitivity achieved with large cluster projectiles; a grand total of 10^4–10^5 projectiles is sufficient for the quantitative detection of SIs. The high detection sensitivity can be applied to track accurately the presence of organics over depth of a few nm with two caveats. The SI spectrum from C_{60}^+ impacts includes a contribution of recoiled projectile constituents sufficient to preclude detection of organics via C^-, CH^-, C_2^- or C_3^-. An unexpected observation is the enhanced ionization of C^- and CH^- occurring with both C_{60}^+ and Au_{400}^{4+}, which is attributed to the presence of metal atoms in the expansion volume. Additional studies with different multilayer films should provide further insight into the efficiency of metal assisted ionization in large projectile impacts.

Acknowledgements

This work is supported by National Science Foundation (CHE-0449312) and R.A. Welch Foundation (A-1482).

References

[1] K. Boussofiane-Baudin, G. Bolbach, A. Brunelle, S. Della-Negra, P. Hakansson, Y. Le Beyec, Nucl. Instrum. Methods B 88 (1994) 160.

[2] E.A. Schweikert, M.J. Van Stipdonk, R.D. Harris, Rapid Comm. Mass Spectrom. 10 (1996) 1987.
[3] D. Weibel, S. Wong, N. Lockyer, P. Blenkinsopp, R. Hill, J.C. Vickerman, Anal. Chem. 75 (2003) 1754.
[4] A. Tempez, J.A. Schultz, S. Della-Negra, J. Depauw, D. Jacquet, A. Novikov, Y. Lebeyec, M. Pautrat, M. Caroff, M. Ugarov, H. Bensaoula, M. Gonin, K. Fuhrer, A. Woods, Rapid Comm. Mass Spectrom. 18 (2004) 371.
[5] J.E. Locklear, S.V. Verkhoturov, E.A. Schweikert, Int. J. Mass Spectrom. 238 (2004) 59.
[6] N. Winograd, Anal. Chem. 77 (2005) 143A.
[7] R.D. Rickman, S.V. Verkhoturov, G.J. Hager, E.A. Schweikert, Int. J. Mass Spectrom. 245 (2005) 48.
[8] Z. Li, S.V. Verkhoturov, E.A. Schweikert, Anal. Chem. 78 (2006) 7410.
[9] G. Decher, Science 277 (1997) 1232.
[10] Y. Zhou, Z. Li, N. Hu, Y. Zeng, J.F. Rusling, Langmuir 18 (2002) 8573.
[11] A. Delcorte, B.J. Garrison, Nucl. Instrum. Methods B 255 (2007) 223.
[12] C. Anders, H. Kirihata, Y. Yamaguchi, H.M. Urbassek, Nucl. Instrum. Methods B 255 (2007) 247.
[13] J.E. Locklear, Ph.D. Dissertation, Texas A&M University, College Station, TX, 2006.
[14] J.E. Locklear, C. Guillermier, S.V. Verkhoturov, E.A. Schweikert, Appl. Surf. Sci. 252 (2006) 6624.
[15] R.D. Rickman, Ph.D. Dissertation, Texas A&M University, College Station, TX, 2004.
[16] R. Holm, S. Storp, Surf. Interface Anal. 2 (1980) 96.
[17] Y. Lvov, G. Decher, H. Mohwald, Langmuir 9 (1993) 481.
[18] W. Harbich, in: K.H. Meiwes-Broer (Ed.), Metal Clusters at Surfaces: Structure, Quantum Properties, Physical Chemistry, Springer, Berlin, 2000, p. 123.
[19] C.W. Diehnelt, M.J. Van Stipdonk, E.A. Schweikert, Nucl. Instrum. Methods B 142 (1998) 606.
[20] M.H. Shapiro, T.A. Tombrello, Phys. Rev. Lett. 68 (1992) 1613.
[21] A. Delcorte, S. Yunus, N. Wehbe, N. Nieuwjaer, C. Poleunis, A. Felten, L. Houssiau, J.J. Pireaux, P. Bertrand, Anal. Chem. 79 (2007) 3673.